Inorg. Chem. **2002**, *41*, 5686–5692

Unusual Magnetic Properties of One-Dimensional Molecule-Based Magnets Associated with a Structural Phase Transition

Xiaoming Ren, Qingjin Meng,* You Song, Changsheng Lu, and Chuanjiang Hu

Coordination Chemistry Institute, State Key Laboratory of Coordination Chemistry, Nanjing University, Nanjing 210093, P.R. China

Xiaoyuan Chen

Department of Chemistry, Syracuse University, Syracuse, New York 13244

Received November 13, 2001

Three ion-pair complexes, $[RbzPy]^+[Ni(mnt)_2]^-$ (mnt^{2-} = maleonitriledithiolate; $[RbzPy]^+$ = 4-R-benzylpyridinium; R = Br (**1**), Cl (**2**), and NO_2 (**3**)), with unusual magnetic properties have been synthesized and characterized. The crystal structures of **1** and **2** have been solved. The two complexes belong to the $P2_1/c$ space group with $Z = 4$ and $C_{20}H_{11}BrN_5NiS_4$, $a = 12.0744(17)$ Å, $b = 26.369(4)$ Å, $c = 7.440(3)$ Å, and $\beta = 102.63(3)°$ for **1** and $C_{20}H_{11}ClN_5NiS_4$, $a = 12.105(2)$ Å, $b = 26.218(4)$ Å, $c = 7.374(2)$ Å, and $\beta = 102.55(2)°$ for **2**, respectively. The $[Ni(mnt)_2]^-$ anions in **1**–**3** form uniformly spaced one-dimensional (1-D) magnetic chains of $s = 1/2$ at room temperature. The temperature dependences of the susceptibility for **1**–**3** show that they undergo phase transitions. All three complexes are paramagnetic in their high-temperature (abbreviation HT) phase and diamagnetic in the low-temperature (abbreviation LT) phase because of strong dimerization along the stacking direction. The results of thermal analysis (DSC) further confirm that the phase transition for **1** and **2** is first-order but maybe second-order for **3**. The phenomena observed in this study are similar to those of the 1-D radical systems.

Introduction

Recently, quasi-one-dimensional compounds have attracted widespread attention because they show novel physical properties such as Peierls transitions, spin-Peierls transitions, charge-density-wave (CDW) states, spin-density-wave (SDW) states, superconductivity, molecular bistability, molecular magnetic nanowire properties, etc.[1–5] In addition, 1-D compounds have stimulated theoretical investigations.

One of the most studied classes of 1-D transition metal complexes is the complexes containing $[M(mnt)_2]^-$ (M = Ni(III), Pd(III), or Pt(III); mnt^{2-} = maleonitriledithiolate) ion. In these compounds, the constituent planar molecules $[M(mnt)_2]^-$ form columnar stack structures, in which intermolecular d_{z^2} or π orbital interaction result in 1-D electronic nature.[6–9] Usually, the topology and size of the countercation in $[M(mnt)_2]^-$ complexes may play an important role in controlling the stacking of anions and cations. We have recently developed a new class of salts $[Cat]^+[Ni(mnt)_2]^-$ ($[Cat]^+$ = benzylpyridinium derivatives) that may be described as structurally and magnetically 1-D molecular solids due to the cations being nonplanar. Furthermore, the stacking structure of these complexes can be finely tuned by systematically varying the substituents in the aromatic

* To whom correspondence should be addressed. E-mail: MengQJ@netra.nju.edu.cn.

(1) Coomber, A. T.; Beljonne D.; Friend, R. H.; Brédas, J. L.; Charlton, A.; Robertson, N.; Underhill, A. E.; Kurmoo, M.; Day, P. *Nature* **1996**, *380*, 144.
(2) Manabe, T.; Kawashima, T.; Ishii, T.; Matsuzaka, H.; Yamashita, M.; Mitani, T.; Okamoto, H. *Synth. Met.* **2001**, *116*, 415.
(3) Wei, J. H.; Zhao, J. Q.; Liu, D. S.; Xie, S. J.; Mei, L. M.; Hong, J. *Synth. Met.* **2001**, *122*, 305.
(4) (a) Sugano, T. *Polyhedron* **2001**, *20*, 1285 and the references therein. (b) Kommandeur, J.; Vegter, J. G. *Mol. Cryst. Liq. Cryst.* **1975**, *30*, 11. (c) Kosaki, A.; Sorai, M.; Suga, H.; Seki, S. *Bull. Chem. Soc. Jpn.* **1977**, *50*, 810. (d) Fujita, W.; Awaga, K. *Science* **1999**, *286*, 261.
(5) Caneschi, A.; Gatteschi, D.; Lalioti, N.; Sangregorio, C.; Sessoli, R.; Venturi, G.; Vingingni, A.; Rettori, A.; Pini, M. G.; Novak, M. A. *Angew. Chem., Int. Ed.* **2001**, *40*, 1760.
(6) Nishijo, J.; Ogura, E.; Yamaura, J.; Miyazaki, A.; Enoki, T.; Takano, T.; Kuwatani, Y.; Iyoda, M. *Solid State Commun.* **2000**, *116*, 661.
(7) Pullen, A. E.; Faulmann, C.; Pokhodnya, K. I.; Cassoux, P.; Tokumoto, M. *Inorg. Chem.* **1998**, *37*, 6714.
(8) Allan, M. L.; Coomber, A. T.; Marsden, I. R.; Martens, J. H. F.; Friend, R. H.; Charlton, A.; Underhill A. E. *Synth. Met.* **1993**, *55*−*57*, 3317.
(9) Kobayashi, A.; Sasaki, Y.; Kobayashi, H.; Underhill, A. E.; Ahmad, M. M. *J. Chem. Soc., Dalton Trans.* **1982**, 390.

10.1021/ic0111637 CCC: $22.00
Published on Web 10/03/2002

Chart 1

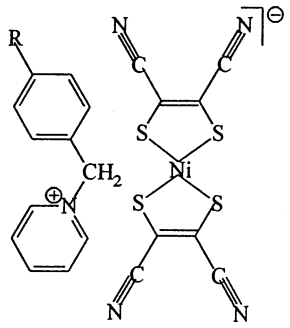

rings.[10,11] In this paper, we report the structures and unusual magnetic properties of three quasi-one-dimensional molecule-based magnets formed by $[Ni(mnt)_2]^-$ anions and benzylpyridinium derivatives $[RbzPy]^+$ (Chart 1).

Experimental Section

General Methods. The starting materials Na_2mnt and [RbzPy]-Cl were synthesized by literature procedures.[12,13] A method similar to that for preparing $[Bu_4N]_2[Ni(mnt)_2]$ was used to prepare $[RbzPy]_2[Ni(mnt)_2]$.[12]

Preparation of [BrbzPy][Ni(mnt)$_2$] (1). A MeCN solution (10 cm^3) of I_2 (150 mg, 0.59 mmol) was slowly added to a MeCN solution (20 cm^3) of $[BrbzPy]_2[Ni(mnt)_2]$ (813 mg, 1.0 mmol), and the mixture was stirred for 15 min. MeOH (90 cm^3) was then added. The mixture was allowed to stand overnight, and then 500 mg of brown-red microcrystals was filtered off, washed with MeOH, and dried in a vacuum. Yield: 85%. Anal. Calcd for $C_{20}H_{11}BrN_5NiS_4$: C, 40.84; H, 1.89; N, 11.91; Ni, 9.98. Found: C, 40.55; H, 1.96; N, 11.63; Ni, 9.76. IR spectrum (cm^{-1}): ν(CN), 2206 s, 2156 sh; ν(C═C) of mnt^{2-}, 1456 m.

Preparations of [ClbzPy][Ni(mnt)$_2$] (2) and [NO$_2$BzPy][Ni(mnt)$_2$] (3). The same procedure used for preparing **1** was also used to synthesize **2** and **3**. Yield of **2**: 86%. Anal. Calcd for $C_{20}H_{11}ClN_5NiS_4$: C, 44.18; H, 2.04; N, 12.88; Ni, 10.79. Found: C, 44.10; H, 2.11; N, 12.64; Ni, 10.67. IR spectrum (cm^{-1}): ν(CN), 2206 s, 2154 sh; ν(C═C) of mnt^{2-}, 1456 m. Yield of **3**: 82%. Anal. Calcd for $C_{20}H_{11}N_6NiO_2S_4$: C, 43.34; H, 2.00; N, 15.16; Ni, 10.59. Found: C, 43.21; H, 2.44; N, 14.98; Ni, 10.51. IR spectrum (cm^{-1}): ν(CN), 2208 s, 2158 sh; ν(C═C) of mnt^{2-}, 1456 m.

All single crystals suitable for X-ray structure analyses were obtained by evaporating solutions of **1** or **2** in mixtures of MeCN and *n*-PrOH (1:1 v/v).

Physical Measurements. Elemental analyses for C, H, and N were performed with a Perkin-Elmer 240 analytical instrument, Ni analysis was made on a Shimadzu AA-680 atomic absorption-flame emission spectrophotometer, and Br, Cl, O, and S analyses were not carried out. IR spectra (KBr pellets) in the 4000−400 cm^{-1} regions were obtained on a IFS66V FT-IR spectrophotometer. Magnetization measurements were carried out with a Quantum Design MPMS-5S superconducting quantum interference device (SQUID) magnetometer, and the diamagnetic corrections of a sample for the constituent atoms were made with Pascal's constants. DSC experiments were performed with a Perkin-Elmer calorimeter. Thermal analysis of polycrystalline samples placed in an aluminum crucible was carried out on warming (rate of 20 K min^{-1}) in the temperature range of −180 to 20 °C (93−293 K).

X-ray Crystallography. The crystal structures of **1** and **2** were determined at room temperature with a Siemens P4 four-circle diffractometer. All computations were carried out on a PC-586 computer using the SHELXTL-PC program package.[14] The structures were solved by direct method and refined on F^2 by the full-matrix least-squares method. All non-hydrogen atoms were refined anisotropically. Hydrogen atoms were placed in their calculated positions and refined by following the riding model. Other details of crystal data collection and refinement are listed in Table 1.

Results and Discussion

Crystal Structures. [BrbzPy][Ni(mnt)$_2$] (**1**) crystallizes in the monoclinic space group $P2_1/c$ at room temperature. For $[Ni(mnt)_2]^-$ anions, the nickel atom exhibits square-planar coordination geometry with four sulfur atoms. The average S−Ni−S bond angle (92.27(9)°) within the five-membered ring and the average Ni−S bond distance (2.145-(2) Å) agree well with those found in other $[Ni(mnt)_2]^-$ complexes.[15] The cation, $[BrbzPy]^+$, adopts a conformation in which the benzene and pyridine rings are almost perpendicular to the reference plane C(12)−C(15)−N(5) (dihedral angles of 97.3 and 93.3°, respectively).

The most prominent structural features of **1** are the completely segregated stacks of anions and cations (Figure 1 a). Furthermore, the $[Ni(mnt)_2]^-$ anions are uniformly spaced along the columns as depicted in Figure 1b. The nearest S···S, S···Ni, and Ni···Ni distances within the columns are 3.74, 3.64, and 3.93 Å, respectively. The shortest Ni···Ni contact between $[Ni(mnt)_2]^-$ columns is 11.90 Å.

In Figure 2, other prominent structural features of **1** involve the packing of the $[BrbzPy]^+$ cations; similar phenomena have been found in some halogenbenzene derivatives in the solid state[16] owing to p−π interactions between halogen atoms and benzene rings. The benzene rings are parallel with respect to each other. The contact distances of Br(1) atoms to neighboring benzene rings are 3.64 Å for C(9)C(10)-C(11)C(12)C(13)C(14) (x, 1.5 − y, 0.5 + z) and 3.77 Å for C(9)C(10)C(11)C(12)C(13)C(14) (x, 1.5 − y, −0.5 + z), respectively. These contacts are almost identical with the sum of the van der Waals radies of Br and the half thickness of an aromatic ring (3.70 Å). The cations form 1-D chains via p−π interactions between Br atoms and benzene rings.

[ClbzPy][Ni(mnt)$_2$] (**2**) (as shown in Table 1) and [NO$_2$-bzPy][Ni(mnt)$_2$] (**3**)[11] are isostructural with **1** at room temperature; the coordination geometry of the Ni(III) ions and stacking patterns of both anions and cations in **2** and **3** are essentially identical to those described above for **1**. Selected bond distances, bond angles, and intermolecular Ni···Ni, Ni···S, and S···S distances are summarized in Table 2. For **2**, the neighboring benzene rings within $[ClbzPy]^+$

(10) Ren, X. M.; Lu, C. S.; Liu, Y. J.; Zhu, H. Z.; Li, H. F.; Hu, C. J.; Meng, Q. J. *Transion Met. Chem.* **2001**, *26*, 136.
(11) Zhu, X. H.; You, X. Z.; Ren, X. M.; Tan, W. L.; Dai, W.; Raj, S. S. S.; Fun, H. K. *Chem. Lett.* **2000**, 472.
(12) Davison, A.; Holm, H. R. *Inorg. Synth.* **1967**, *10*, 8.
(13) Bulgarevich, S. B.; Bren, D. V.; Movshovic, D. Y.; Finocchiaro, P.; and Failla, S. *J. Mol. Struct.* **1994**, *317*, 147.
(14) Sheldrick, G. M. *SHELXTL, Structure Determination Software Programs*, version 5.10; Bruker Analytical X-ray Systems Inc.: Madison, WI, 1997.
(15) Brunn, K.; Endres, H.; Weiss, J. *Z. Naturforsch.* **1987**, *42B*, 1222.
(16) (a) Sundberg, M. R. *Inorg. Chim. Acta* **1998**, *267*, 249. (b) Sillanpää, R.; Jokela, J.; Sundberg, M. R. *Inorg. Chim. Acta* **1997**, *258*, 221. (c) Sundberg, M. R.; Sillanpää, R. *Acta Chem. Scand.* **1992**, *46*, 34.

Table 1. Crystal Data and Structure Refinement for **1** and **2**

param	**1**	**1**[17]	**2**
temp/K	293(2)	89(2)	293(2)
empirical formula	$C_{20}H_{11}BrN_5NiS_4$	$C_{20}H_{11}BrN_5NiS_4$	$C_{20}H_{11}ClN_5NiS_4$
fw	588.20	588.20	543.74
wavelength/Å	0.710 73	0.710 73	0.710 73
cryst system	monoclinic	triclinic	monoclinic
space group	$P2_1/c$	$P\bar{1}$	$P2_1/c$
unit cell dimens			
a/Å	12.0744(17)	7.238(4)	12.105(2)
b/Å	26.369(4)	12.006(6)	26.218(4)
c/Å	7.440(3)	26.075(13)	7.374(2)
α/deg	90	88.469(10)	90
β/deg	102.63(3)	86.755(9)	102.55(2)
γ/deg	90	77.476(9)	90
V/Å^3, Z	2311.4(12), 4	2208.2(19), 4	2284.2(9), 4
D(calcd)/(g/cm^3)	1.690	1.769	1.581
ab coeff/mm^{-1}	2.948	3.085	1.350
F(000)	1172	1172	1100
cryst size/mm^3	0.4 × 0.2 × 0.2	0.4 × 0.4 × 0.12	0.6 × 0.4 × 0.4
θ range for data collcn/deg	1.89−24.99	1.74−28.37	1.89−25.00
limiting indices	$-14 \le h \le 14$	$-9 \le h \le 9$	$-14 \le h \le 14$
	$-31 \le k \le 1$	$-16 \le k \le 13$	$-31 \le k \le 1$
	$-1 \le l \le 8$	$-34 \le l \le 32$	$-1 \le l \le 8$
reflcns collcd	5240	14755	5200
indpdt reflcns	4028 (R_{int} = 0.0740)	10 172 (R_{int} = 0.0757)	3997 (R_{int} = 0.0455)
abs corr	ψ scan	none	ψ scan
max and min transm	0.4830 and 0.2991		0.5492 and 0.4004
refinement method		full-matrix least- squares on F^2	
data/restraints/params	4028/0/281	10172/0/560	3997/0/294
goodness-of-fit on F^2	1.013	3.676	1.023
Final R indices [$I > 2\sigma(I)$][a]	R1 = 0.0717	R1 = 0.2181	R1 = 0.0460
	wR2 = 0.1765	wR2 = 0.5472	wR2 = 0.1065
R indices (all data)[a]	R1 = 0.1262	R1 = 0.2486	R1 = 0.0773
	wR2 = 0.2152	wR2 = 0.5543	wR2 = 0.1226
largest diff peak and hole/e Å^{-3}	0.892 and 1.192	5.624 and 3.885	0.457 and 0.426

[a] $R1 = \Sigma(||F_o| - |F_c||)/\Sigma|F_o|$, $wR2 = \Sigma w(|F_o|^2 - |F_c|^2)^2/\Sigma w(|F_o|^2)^2]^{1/2}$.

Table 2. Selected Bond Parameters and Intermolecular Contacts for **1**−**3**

	1 (293 K)	**1** (89 K)[17]	**2** (293 K)	**3** (293 K)[11]
Bond Dstances (Å)				
Ni(1)−S(1)	2.141(2)	2.130(6)	2.1447(12)	2.144(2)
Ni(1)−S(2)	2.148(2)	2.146(6)	2.1392(12)	2.148(2)
Ni(1)−S(3)	2.140(2)	2.146(6)	2.1510(12)	2.141(2)
Ni(1)−S(4)	2.152(2)	2.149(6)	2.1395(12)	2.156(2)
Ni(2)−S(5)		2.126(6)		
Ni(2)−S(6)		2.131(6)		
Ni(2)−S(7)		2.154(6)		
Ni(2)−S(8)		2.137(6)		
Bond Angles (deg)				
S(1)−Ni(1)−S(2)	92.11(9)	93.1(2)	92.17(5)	92.2(1)
S(1)−Ni(1)−S(3)	85.96(9)	89.3(2)	89.40(5)	85.9(1)
S(3)−Ni(1)−S(4)	92.43(9)	92.1(2)	92.37(5)	92.5(1)
S(2)−Ni(1)−S(4)	89.57(9)	85.4(2)	86.01(5)	89.3(1)
S(5)−Ni(2)−S(6)		92.8(2)		
S(5)−Ni(2)−S(7)		89.1(2)		
S(6)−Ni(2)−S(8)		85.4(2)		
S(7)−Ni(2)−S(8)		92.5(2)		
Intrachain Distances (Å)				
Ni···Ni (nearest separation)	3.93	3.65, 3.85	3.91	3.83
Ni···S (<3.7 Å)	3.64	3.57	3.63, 3.63	3.61, 3.61
S···S (<3.7 Å)		3.51		3.67
Interchain Distances (Å)				
Ni···Ni (nearest separation)	11.90	11.82	11.94	11.99

cations column are parallel. The contact distances of Cl(1) atom to neighbor benzene rings are 4.00 Å for C(9)C(10)-C(11)C(12)C(13)C(14) (x, 1.5 − y, −0.5 + z) and 3.81 Å for C(9)C(10)C(11)C(12)C(13)C(14) (x, 1.5 − y, 0.5 + z), respectively. These values are larger than the contacts between Br and benzene rings observed in **1**; obviously, the stacking interactions between cations in **2** are weaker than that in **1**. For **3**, the NO_2 group and the benzene ring in the $[NO_2bzPy]^+$ cation are almost coplanar; the dihedral angle between the two planes is 3.8°. The benzene rings of neighboring cations are parallel. Compared with **1** and **2**, there are more atoms with shorter contacts for **3**; therefore, it is possible that the stacking interactions between cations in **3** may be stronger than in **1** or **2**.

Crystal Structure of 1 at 89 K.[17] Crystals of **1** at 89 K show the space group of $P\bar{1}$, different from $P2_1/c$ at room temperature. Due to symmetry lowering, the numbers of ion-pair molecule in the asymmetric unit of a cell increases from one at room temperature to two at 89 K. Although the average S−Ni−S bond angles of 92.6(3) and 92.7(3)° within

(17) Note: The structure of **1** in the LT phase was measured by a CCD area detector at 89 K. Crystallographic data: $C_{20}H_{11}BrN_5NiS_4$, space group $P\bar{1}$, a = 7.238(4) Å, b = 12.006(6) Å, c = 26.075(13) Å, α = 88.469(10)°, β = 86.755(9)°, γ = 77.476(9)°, V = 2208.2(19) Å^3, Z = 4, R = 0.2192. There are two $[Ni(mnt)_2]^-$ anions in an asymmetric unit at 89 K. Although the average Ni−S bond distances are in agreement with the values at room temperature, all the intermolecular S···S, S···Ni, and Ni···Ni contacts at 89 K are observed to be significantly shorter than in the corresponding room-temperature structure. The nearest distances are S···S of 3.51 Å, S···Ni of 3.57 Å, and Ni···Ni of 3.65 and 3.85 Å within the $[Ni(mnt)_2]^-$ stacking column, respectively. The shortest Ni···Ni contact between $[Ni(mnt)_2]^-$ anions of the intercolumns is 11.82 Å. The uniformly spaced 1-D anion chains at room temperature dimerize obviously in the low-temperature phase and become alternating chains.

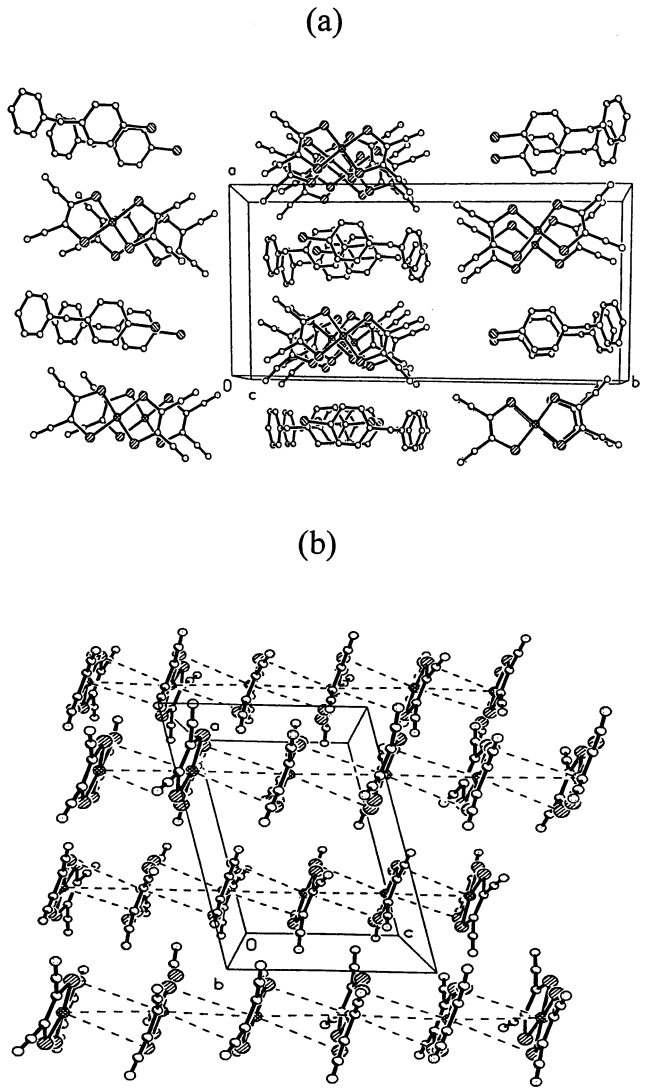

Figure 1. (a) Stack of anions and cations of **1** along the *c*-axis and (b) $[Ni(mnt)_2]^-$ anion chains with equal Ni···Ni distant viewing along the *b*-axis (at room temperature).

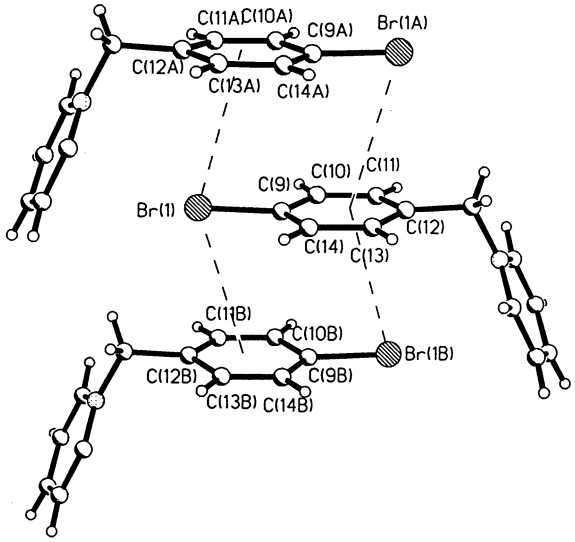

Figure 2. Br−π interactions between Br atoms and benzene rings for **1**.

the five-membered ring and the average Ni−S bond distances of 2.143(6) and 2.137(6) Å agree with the values at room

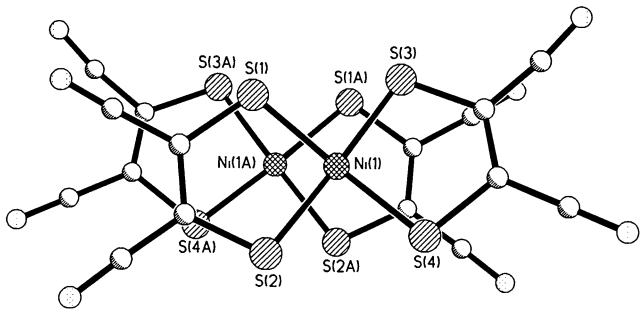

Figure 3. Models of overlapping of $[Ni(mnt)_2]^-$ anions for **1** in the HT phase.

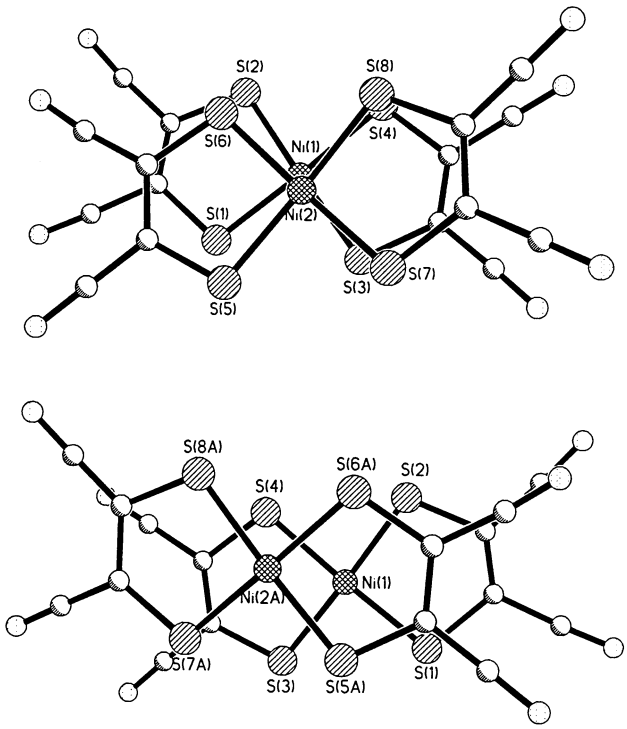

Figure 4. Models of overlapping of $[Ni(mnt)_2]^-$ anions for **1** in the LT phase.

temperature, all intermolecular S···S, S···Ni, and Ni···Ni contacts at 89 K are significantly shorter than those of the corresponding room-temperature structure. The nearest S···S distances are 3.51 Å, S···Ni = 3.57 Å, and Ni···Ni = 3.65 and 3.85 Å, all within the $[Ni(mnt)_2]^-$ stacks. The shortest Ni···Ni contact between columns is 11.82 Å. The contact distances between bromine atoms and neighboring benzene rings are 3.48 and 3.63 Å, respectively. These intermolecular contacts become shorter at low temperature and are associated with a reduction of the cell volume from 2311.4(12) Å^3 at room temperature to 2208.2(19) Å^3 at 89 K. The overlap of the $[Ni(mnt)_2]^-$ ions in the LT phase are different from that in HT phase (Figures 3 and 4). The uniformly spaced anions in the HT phase dimerize in the LT phase and form alternating chains (Figure 5).

Magnetic Properties. The temperature dependence of the magnetic susceptibility for **1**−**3** was measured in the temperature range 2−300 K, with an applied field of 10 kOe. For three samples, their variable-temperature magnetic moments ($M(T)$) were measured in different sample mass (m) for two times; that is, $M_1(T)$ for m_1 and $M_2(T)$ for m_2.

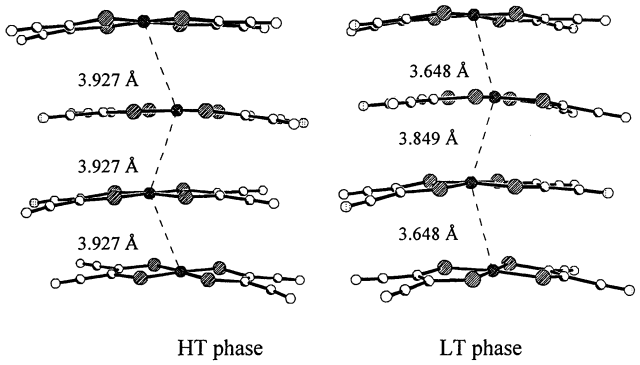

Figure 5. Side view of 1-D anion chain for **1** in the HT and LT phases.

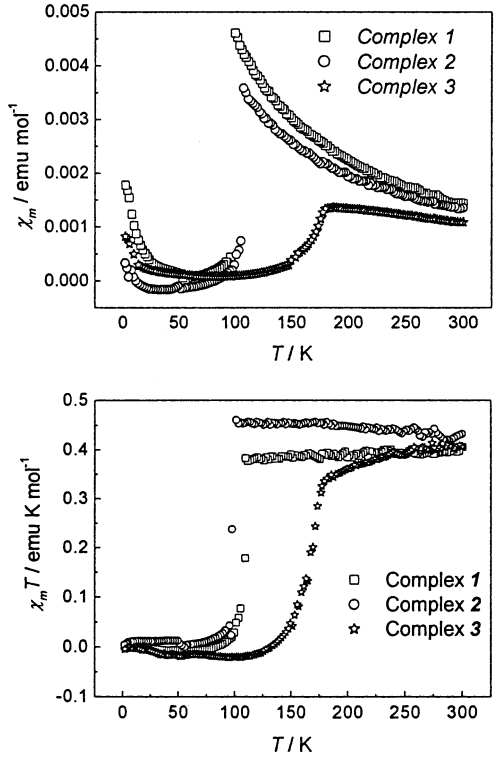

Figure 6. Plots of χ_m-T (top) and χ_mT-T (bottom) of **1**−**3**.

Due to M(practically measured) = M(sample) + M(holder and capsule), the diamagnetic contribution of the sample holder and the capsule may be subtracted if the magnetic susceptibility is calculated by the following formula:

$$\chi_m = \frac{\{M_1(T) - M_2(T)\}M_r}{(m_1 - m_2)H}$$

Here M_r represents the formula weight. The plots of χ_m versus T and χ_mT versus T for these three complexes are shown in Figure 6 with χ_m being the molar magnetic susceptibility corrected by the diamagnetic contribution and T being temperature.

For **1**, the overall behavior corresponds to an antiferromagnetically coupled system: χ_mT slightly decreases on cooling from 0.397 emu·K·mol^{-1} at 300 K to 0.378 emu·K·mol^{-1} at 109.6 K and drops sharply around 109.6 K. When the sample temperature is lower than 70 K, the value of χ_mT is close to zero. On increase of the temperature back to the original temperature, the same χ_mT curve is obtained, and no hysteresis effect is detected. At approximately 109.6 K the abrupt drop of the magnetic susceptibility of **1** indicates that **1** undergoes a phase transition. The structural change of the magnetic chain of **1** from the HT (HT) to the LT phase (LT) meets the requirements of a spin-Peierls transition: (1) The magnetic chain is flexible. (2) The magnetic exchange interactions between magnetic chains are negligible compared with those within magnetic chains. This is due to magnetic chains being separated by nonmagnetic organic cation stacks.[18] However, the space group change from $P2_1/c$ in the HT phase to $P\bar{1}$ in the LT phase reveals that the phase transition for **1** may be first-order[19] and not the spin-Peierls transition because the spin-Peierls transition is second-order. A similar phenomenon was observed in a 1-D antiferromagnetically coupled radical system.[4]

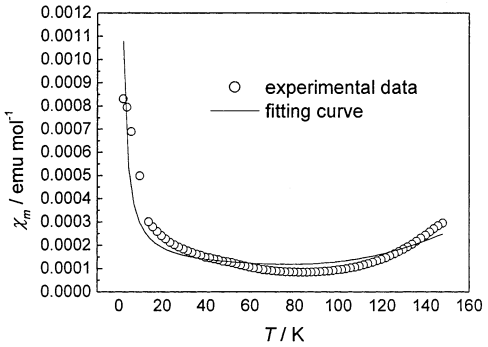

Figure 7. Plots of χ_m versus T below the phase transition temperature for **3**.

The overall magnetic behavior of **3** corresponds to antiferromagnetically coupled system too and is similar to that of **1** (Figure 6). Compared with **1**, the χ_mT values of **3** in the HT phase decrease faster than that of **1** as the sample temperature cooled, and the inflection point is not as abrupt as that of **1**. The phase transition temperature showed in the plot of χ_mT versus T is around 181.7 K. Below the transition temperature, the magnetic susceptibility of this complex gradually decreases with decreasing temperature to indicate the magnetic susceptibility being activated,[20] so the magnetic susceptibility may be fitted by $\chi_m = [\alpha(1 - P)\exp(-\Delta/k_BT)]/T + PNg^2\mu_B^2/(4k_BT) + \chi_0$, where α is a constant value corresponding to the dispersion of excitation energy, Δ is the magnitude of the spin gap, P is the uncoupling impurities content, χ_0 is the constant term caused by Van Vleck paramagnetism, and other signs have their usual meaning. The best fit curve is displayed in Figure 7, and the corresponding parameters are given as following: $g = 2.12$; $P = 0.005$; $\alpha = 3.2$; $\Delta/k_B = 738.3$ K; $\chi_0 = 0.00009$ emu mol^{-1}; agreement factor $R = 1.1 \times 10^{-3}$ [R is defined as $\Sigma_i(\chi_m^{calc} - \chi_m^{obd})^2/(\chi_m^{obd})^2$]. The obtained value of the parameter, $2\Delta/k_BT_{SP}$ (T_{SP} is the transition temperature of 181.7 K), is 8.13 and more removed from the ideal value of 3.53 derived using the BCS formula in a weak coupling

(18) Kahn, O. *Molecular Magnetism*; VCH: New York, 1993; p 269.
(19) König, E.; Ritter, G.; Kulshreshtha, S. K. *Chem. Rev.* **1985**, *85*, 219.
(20) Isett, L. C.; Rosso, D. M.; Bottger, G. L. *Phys. Rev. B* **1980**, *22*, 4739.

regime. These results mean that the short-range magnetic correlations within the chain are not fully developed and intrinsic magnetoelastic instability of a 1-D system cannot be considered as a driving force for the transition; namely, the transition is not a pure spin-Peierls transition but an exotic one.

The magnetic exchange behavior of **2** in the HT phase is different from that of **1** and **3**; the $\chi_m T$ values increase little by little as the sample was cooled (Figure 6), and it reveals that there exist weak ferromagnetic coupled interactions between neighboring Ni(III) ions. When the sample temperature cools to around 101.7 K, the $\chi_m T$ values drop abruptly. Subsequently, the magnetic behavior of **2** is similar to that of **1** and **3**, and when the sample temperature is lower than 70 K, the value of $\chi_m T$ of **2** almost tends to zero. It is worthy of noting that the magnetic exchange properties of **1**−**3** in the HT phase are different although all of the three complexes show uniformly 1-D spaced chain structure. As for containing the $[Ni(mnt)_2]^-$ anion complex, the previous studies have shown that the magnetic coupling between $[Ni(mnt)_2]^-$ anions is very sensitive to not only intermolecular separation[1] but also overlap fashion of neighboring $[Ni(mnt)_2]^-$ anions.[6,21] The theoretic studies also indicated that no simple correlation of magnetic coupling is possible with few structural parameters due to extensive delocalization of the electron density in the $[Ni(mnt)_2]^-$ unit, and several shorter contact distances, such as Ni···Ni, Ni···S, S···S, S···N, S···C, and C···N, play significant roles in the superexchange pathway.[22] Therefore, the different magnetic exchange features between the three complexes may be understood.

Thermodynamic Properties. DSC measurements on these complexes were performed to obtain additional information about the thermodynamic properties of these phase transitions. The power-compensated DSC traces at a warming rate of 20 K·min^{-1} are displayed in Figure 8. Clearly, **1** and **2** have similar thermodynamics and show abruptly endothermic peaks in their DSC traces. The phase transition temperatures obtained from thermal analyses for these two complexes are 113.5 K (−159.5 °C) for **1** and 106.4 K (−166.6 °C) for **2**, respectively, and these values are near the results obtained from magnetic susceptibility measurements. The endothermic enthalpy changes (ΔH), which were calculated from the peak areas, are 444.1 J·mol^{-1} for **1** and 514.9 J·mol^{-1} for **2**, respectively. Therefore, the results of thermal analysis of **1** and **2** further confirm that the phase transitions observed are first-order.[23] However, the thermal behavior of **3** is largely different from that of **1** and **2**; there is not a clear endothermic peak and only baseline shift around the phase transition temperature in the DSC trace. The baseline shift indicates the second-order phase transition[24] and suggests the existence

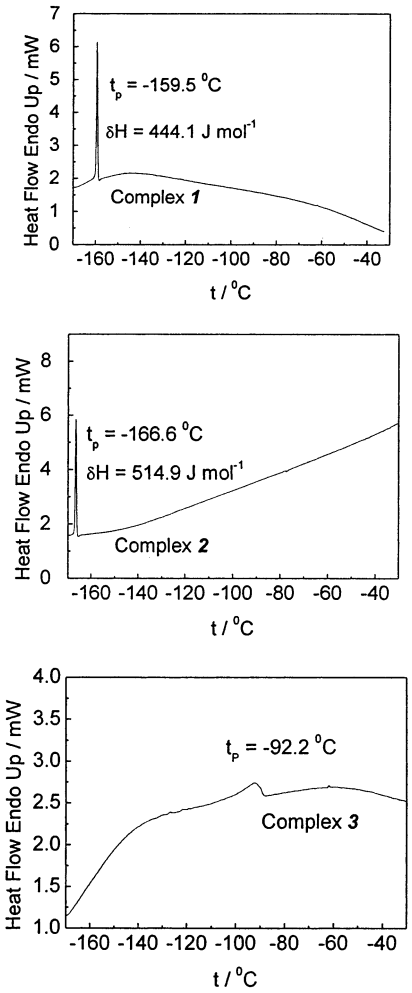

Figure 8. DSC curves of complexes **1**−**3** showing t_p and δH of the phase transitions.

of a possible spin-Peierls transition. The corresponding phase transition temperature obtained from DSC analysis is 180.3 K (−92.2 °C); to our best knowledge, the observed critical temperature is the highest among spin-Peierls organic and organic compounds at present.

Conclusions

The crystal structures at room temperature of three ion-pair complexes reveal uniformly spaced 1-D $[Ni(mnt)_2]^-$ anion chain property arising from a delicate balance among many cooperating interactions, such as nonplanar topology of cations, p−π or π−π interactions between adjacent cations, Ni···S bonding, inter-ring repulsion of $[Ni(mnt)_2]^-$ anion,[25] spin−spin coupling interaction, lattice with magnetic interaction along magnetic chain, lattice with 3-D phonons interaction,[26] and so on. The phase transitions are the result of cooperating interactions described above. We also measured the magnetic susceptibilities of three complexes in the temperature range from 2 to 300 K; the plots of $\chi_m T$−T for

(21) Alvarez, S.; Vicente, R.; Hoffmann, R. *J. Am. Chem. Soc.* **1985**, *107*, 6253.
(22) Ramakrishna, B. L. *Inorg. Chim. Acta* **1986**, *114*, 31.
(23) (a) Hatta, I.; Nakayama, S. *Thermochim. Acta* **1998**, *318*, 21. (b) Jakubas, R.; Clapala, P.; Pietraszko, A.; Zaleski, J.; Kusz, J. *J. Phys. Chem. Solids* **1998**, *59*, 1309. (c) Tang, T.; Gu, K. M.; Cao, Q. Q.; Wang, D. H.; Zhang, S. Y.; Du Y. W. *J. Magn. Magn. Mater.* **2000**, *222*, 110.
(24) Hashimoto, T.; Katsube, T.; Morito, Y. *Solid State Commun.* **2000**, *116*, 129.
(25) Alvarez, S.; Vicente, R.; Hoffman, R. *J. Am. Chem. Soc.* **1985**, *107*, 6253.
(26) Pytte, E. *Phys. Rev. B* **1974**, *10*, 4637.

1−**3** show break points (around 109.6 K for **1**, 101.7 K for **2**, and 181.7 K for **3**). Although there are similar crystal structures in the HT phase for **1**−**3**, the magnetic coupling and thermodynamic properties are different. The phenomena observed in this study are similar to those in the quasi-one-dimensional radical system such as K−Chloranil, galvinoxyl, M−TCNQ (M = Na, K, Rb), and the heterocyclic thiazyl radical. Our results suggest that rational design of new 1-D magnetic systems consisting of an ion-pair complex may provide the analogues of a quasi-one-dimensional radical system based spin bistability, spin-Peierls transition, and so on, and we are actively pursuing this line of research.

Acknowledgment. This project was supported from the National Natural Science Foundation (Grant Nos. 29771017 and 29831010) and the State Education Commission of China. The authors thank Prof. Q. P. Dai and Ms. Z. R. Yuan of the DSC Lab in the Center of Analysis and Determination of Nanjing University for determining DSC data.

Supporting Information Available: X-ray crystallographic data for complexes **1** and **2** (CIF files). This material is available free of charge via the Internet at http://pubs.acs.org.

IC0111637